

# Effect of thermal regime on the seismic response of a dry bridge in a permafrost region along the Qinghai-Tibet Railway

Xiyin Zhang<sup>1,2</sup>, Mingyi Zhang<sup>\*1</sup>, Xingchong Chen<sup>2</sup>, Shuangyang Li<sup>1</sup> and Fujun Niu<sup>1</sup>

<sup>1</sup>State Key Laboratory of Frozen Soil Engineering, Northwest Institute of Eco-Environment and Resources, Chinese Academy of Sciences, Lanzhou 730000, China

<sup>2</sup>School of Civil Engineering, Lanzhou Jiaotong University, Lanzhou 730070, China

(Received August 12, 2016, Revised November 1, 2017, Accepted December 7, 2017)

**Abstract.** Dry bridges have been widely applied in the Qinghai-Tibet Railway (QTR) to minimize the thermal disturbance of engineering to the permafrost. However, because the Qinghai-Tibet Plateau is an area with a high potential occurrence of earthquakes, seismic action can easily destroy the dry bridges. Therefore, a three-dimensional numerical model, with consideration of the soil-pile interactions, is established to investigate the thermal characteristics and their impact on the seismic response of the dry bridge in permafrost region along the QTR. The numerical results indicate that there exist significant differences in the lateral displacement, shear force, and bending moment of the piles in different thermal conditions under seismic action. When the active layer become from unfrozen to frozen state, the maximum displacement of the bridge pile reduces, and the locations of the zero and peak values of the shear force and bending moment also change. It is found that although the higher stiffness of frozen soil confines the lateral displacement of the pile, compared with unfrozen soil, it has an adverse effect on the earthquake energy dissipation capacity.

**Keywords:** numerical analysis; dry bridge; thermal characteristics; soil-pile interaction; seismic response; permafrost region

## 1. Introduction

In China, permafrost regions are about  $2.15 \times 10^6$  km<sup>2</sup>, accounting for about 22.4% of the land area (Jin *et al.* 2000). Many major highways and railways cross these regions. At present, the Qinghai-Tibet Railway (QTR) is the highest and longest plateau railway in the world, of which about 550 km passes through permafrost regions (Lai *et al.* 2009). In addition, about 275 km of the permafrost along the QTR belongs to the “warm permafrost” category, nearly half of which is ice-rich permafrost (Cheng 2003). This permafrost is extremely unstable under the effects of global warming and thermal disturbance caused by engineering. Dry bridges (Fig. 1) is an engineering practice used to improve the stability of the QTR by decreasing the ground temperature, as they can shade the ground, and air can flow freely under them (Cheng *et al.* 2008). 125-km dry bridges were built in the ice-rich and extremely unstable permafrost regions along the QTR, accounting for 22.7% of the length of the railway (Cheng *et al.* 2008). It is well known that the Qinghai-Tibet Plateau is an area with a high potential occurrence of earthquakes. The 14 November, 2001, MS 8.1 West Kunlun Pass Earthquake is a typical example, and featured the longest surface rupture that has occurred in the Qinghai-Tibet Plateau (Xu *et al.* 2002). The seismic-resistant ability of bridges needs to be considered as an



Fig. 1 Photo of a dry bridge along the Qinghai-Tibet Railway

important factor at the design stage (Geng *et al.* 2014, Han *et al.* 2015, Shao *et al.* 2014).

In cold regions, the frozen ground significantly influences the dynamic characteristics and seismic security of bridges (LeBlanc *et al.* 2004). A number of studies of the dynamic responses of bridges in cold regions have been made using different methods. Crowther (1990) presented a design approach to laterally analyze loaded piles embedded in layered frozen soil by using *p-y* curves to model soil and pile interaction. Suleiman *et al.* (2006) investigated the effects of seasonal freezing on the seismic response of integrated bridge column-foundation systems using large-scale outdoor testing. Sriharan *et al.* (2007) investigated the effects of seasonal freezing on the lateral load response of a bridge column supported by a cast-in-drilled-hole foundation shaft under selected cold temperatures, but they did not consider the thermal distribution of the soil layer in

\*Corresponding author, Professor  
E-mail: myzhang@lzb.ac.cn

detail. Xiong and Yang (2008) built a simplified finite element (FE) model of a soil-pile-bridge pier system, and they investigated the effects of seasonally frozen soil on the seismic behavior of the bridge bents by modal and push-over analyses. Wotherspoon *et al.* (2010) developed a numerical model to study the monotonic and cyclic responses of a bridge foundation influenced by structural and soil nonlinearity. In addition, seasonal frost has been found to have a dominating effect over air temperature on the bridge dynamic properties in cold regions, and these effects should be accounted for in seismic design (Yang *et al.* 2007). However, to date, research for analyzing the effect of frozen ground is lacking, and very few studies have considered the effects of the thermal characteristics on the seismic response of dry bridges in cold regions, especially in permafrost regions. Carcione and Seriani (1998) calculated the compressional and shear-wave velocities of permafrost as a function of unfrozen water content and temperature. Yang *et al.* (2011) conducted a comprehensive analytical investigation of the permafrost effects on the seismic site response, and they concluded that it is unacceptable to consider permafrost as bedrock, or ignore its potential effect on the in-site response in the seismic design of bridges. These studies only investigated the permafrost effect on the site response, and they ignored the soil-foundation interaction. Since negative temperatures greatly change the mechanical properties of soil, and then influence the column-foundation systems, these factors must be considered in the seismic design of bridges under cold conditions (Sritharan *et al.* 2007). Che *et al.* (2014) conducted a series of shaking table tests for the small-scale modeling of the pile foundation for soil temperatures of below 0°C around the pile, and the results indicated that the seismic mechanical properties are extremely sensitive to soil temperature. However, the research into the pile-soil-structure for soil temperatures of below 0°C under seismic action is still insufficient.

In this paper, a soil-foundation-structure interaction model is established to investigate the effect of thermal characteristics on the seismic response of a dry bridge in a permafrost region. A typical beam bridge with a pile foundation from the QTR is taken as a case study. A set of ground motions with the different return periods of 72-year (50% probability of exceedance in 50 years), 474-year (10% probability of exceedance in 50 years), and 2475-year (2% probability of exceedance in 50 years) are selected to generate an ensemble of hazard-consistent input motions. From this study, the dynamic responses (i.e., displacement, shear force, and bending moment) of a bridge with a pile foundation in a permafrost region are then investigated by considering the thermal characteristics of the soil layer in different thermal conditions.

## 2 Conceptual model

### 2.1 Heat transfer model

In permafrost regions, the mechanical properties of the active layer, which is the soil layer between the atmosphere

and the permafrost that is subject to seasonal freezing and thawing (Anisimov *et al.* 1997). In addition, global warming and engineering activities also cause the warming of the permafrost around bridges. As a result, the effect of the soil layers on bridge piles can significantly differ in different seasons and years. Therefore, the temperature is a key factor when analyzing the dynamic behavior of bridge piles.

Here, we first analyze the temperature characteristics of the soil-pile system. To simplify the analysis, it is assumed that the soil layers surrounding the bridge piles are homogeneous and isotropic, and that water migration is negligible. Only conduction and the phase transition problem are considered, and thus the heat transfer process in the soil layers and concrete piles can be described as follows

$$\rho C_e \frac{\partial T}{\partial t} = \frac{\partial}{\partial x} \left( \lambda_e \frac{\partial T}{\partial x} \right) + \frac{\partial}{\partial y} \left( \lambda_e \frac{\partial T}{\partial y} \right) + \frac{\partial}{\partial z} \left( \lambda_e \frac{\partial T}{\partial z} \right) + q_v \quad (1)$$

where  $T$  is the temperature;  $t$  is the time;  $\rho$  is the soil density; and  $C_e$  and  $\lambda_e$  are the effective volumetric heat capacity and effective thermal conductivity, respectively.  $q_v$  is the hydration heat of concrete per unit volume, and for the soil layer,  $q_v$  is equal to 0. The rate of heat release per unit volume of concrete  $q_v$  can be determined as

$$q_v(T, t) = cq(T, t) \quad (2)$$

where  $c$  is the amount of cement per unit volume of concrete.

The rate of heat release per unit volume of cement can be written as follows

$$q(T, t) = \frac{\partial Q(T, t)}{\partial t} \quad (3)$$

The heat of hydration can be described by Eq. (4) (Klemczak and Knoppik-Wróbel 2011)

$$Q(T, t) = Q_0 e^{-at_e^{0.5}} \quad (4)$$

where  $a$  is the coefficient related to the type of cement, and  $t_e$  is the equivalent age of the concrete that is given by the equation under a reference temperature  $T_r$

$$t_e = \int_0^t e^{\frac{E_a}{R} \left( \frac{1}{T} - \frac{1}{T_r} \right)} \quad (5)$$

As for the ratio of  $E_a/R$ , it can be experimentally measured, and ranges within the interval of 3000-8000 K for concrete (Cervera *et al.* 2002).

Using the method of sensible heat capacity, it is assumed that the phase changes of the soil layers occur in a range of temperature (Zhang *et al.* 2012), and the effective volumetric heat capacity  $C_e$  and the effective thermal conductivity  $\lambda_e$  can be expressed as

$$C_e = \begin{cases} C_f & T < (T_m - \Delta T) \\ \frac{L_e}{2\Delta T} + \frac{C_f + C_u}{2} & (T_m - \Delta T) \leq T \leq (T_m + \Delta T) \\ C_u & T > (T_m + \Delta T) \end{cases} \quad (6)$$

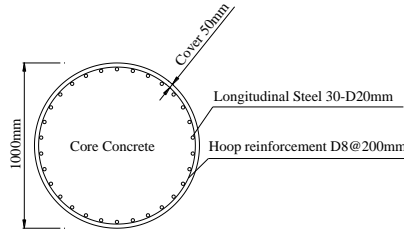


Fig. 2 Section of the pile

$$\lambda_e = \begin{cases} \lambda_f & T < (T_m - \Delta T) \\ \lambda_f + \frac{\lambda_u - \lambda_f}{2\Delta T} [T - (T_m - \Delta T)] & (T_m - \Delta T) \leq T \leq (T_m + \Delta T) \\ \lambda_u & T > (T_m + \Delta T) \end{cases} \quad (7)$$

where  $C_f$  and  $C_u$  are the volumetric heat capacity in the frozen and unfrozen areas, respectively;  $\lambda_f$  and  $\lambda_u$  are the thermal conductivity of the media in the frozen and unfrozen areas, respectively;  $L_s$  is the latent heat of the media;  $T_m - \Delta T$  is the temperature at which the phase change is minimal; and  $T_m + \Delta T$  is the temperature at which the soil is completely thawed.

## 2.2 Governing equation of motion

The governing equation of motion for a bridge can be written as (Wilson 1999)

$$m \frac{d^2 u_a}{dt^2} + c \frac{du_a}{dt} + ku_a = f(t) \quad (8)$$

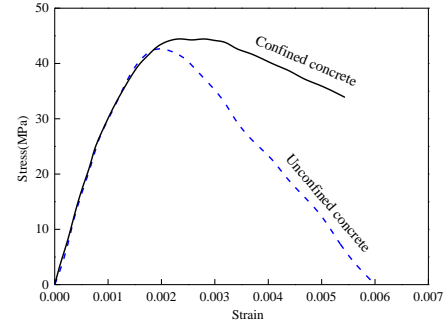
where  $m$ ,  $c$ , and  $k$  are the mass, viscous damping, and static stiffness of the structure, respectively;  $f$  is the external force;  $u_a$  and its time derivatives are the absolute displacement, velocity, and acceleration; and  $t$  is the time.

The basic seismic motions are the three components of the free-field ground displacements  $u(t)_g$  that are known at some point below the foundation level of the structure. Therefore, the absolute displacement, velocity, and acceleration in Eq. (8) can be written in terms of the three components of the free-field ground displacement, velocity, and acceleration

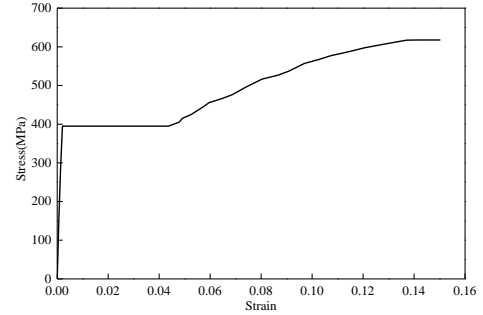
$$\begin{cases} u_a(t) = u(t) + I_x u_{xg}(t) + I_y u_{yg}(t) + I_z u_{zg}(t) \\ \frac{du_a(t)}{dt} = \frac{du(t)}{dt} + I_x \frac{du_{xg}(t)}{dt} + I_y \frac{du_{yg}(t)}{dt} + I_z \frac{du_{zg}(t)}{dt} \\ \frac{d^2 u_a(t)}{dt^2} = \frac{d^2 u(t)}{dt^2} + I_x \frac{d^2 u_{xg}(t)}{dt^2} + I_y \frac{d^2 u_{yg}(t)}{dt^2} + I_z \frac{d^2 u_{zg}(t)}{dt^2} \end{cases} \quad (9)$$

where  $I_i$  ( $i=x, y$  or  $z$ ) is a value of one in the “ $i$ ” directional degrees of freedom and zero in all other positions. The substitution of Eq. (9) into Eq. (8) allows the node point equilibrium equations to be rewritten as

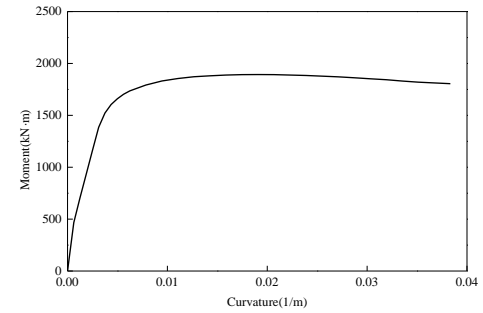
$$m \frac{d^2 u}{dt^2} + c \frac{du}{dt} + ku = -m_x \frac{\partial^2 u_{xg}}{\partial t^2} - m_y \frac{\partial^2 u_{yg}}{\partial t^2} - m_z \frac{\partial^2 u_{zg}}{\partial t^2} \quad (10)$$



(a) Confined and unconfined concrete



(b) Steel bar

 Fig. 3 Constitutive model of the materials ( $T > 0^\circ\text{C}$ )

 Fig. 4 Moment-curvature relationships of the pile sections ( $T > 0^\circ\text{C}$ )

where  $m_i = mI_i$ .

## 2.3 Soil-pile interaction model

For the bridge pile, a longitudinal steel reinforcement ratio of 1.2% is used, the spacing of the transverse steel is 200 mm. The corresponding reinforcement details are shown in Fig. 2.

The pile element has nonlinear but elastic behavior, and which has cracked section properties that are calculated from the moment-curvature analysis by the fiber section model. The tension capacity of the concrete is assumed to be zero for both the confined and unconfined concrete. The following stress-strain curves are used to define the fibers in the inelastic fiber sections for longitudinal column reinforcement, unconfined concrete, and confined concrete, as shown in Fig. 3.

Using the properties of concrete and reinforcement at the appropriate temperatures, the moment-curvature relationships of the pile sections are determined using fiber

section analyses. The moment-curvature curve is shown in Fig. 4.

To analyze the effect of the freeze-thaw state of the soil layers on the dynamic response of the dry bridge, the Winkler beam model (Allotey and El Naggar 2008), as a soil-pile interaction model, is introduced to describe the relationship between the thermal distribution and the dynamic properties of the soil-pile system. The “*p-y* method”, a version of the Winkler model, is commonly used in seismic analysis, in which the soil characteristics in the soil-pile interaction are described by nonlinear resistance-displacement curves, which are known as *p-y* curves. It has been confirmed that the *p-y* approach is effective in predicting the dynamic response of piles to the lateral spreading of the seismic effect in frozen ground crust (Ge *et al.* 2012, Yang and Zhang 2012).

The nonlinear response of the soil is modeled in the analysis by characterizing the response of the lateral soil spring, with appropriate *p-y* curves, as a function of depth and temperature (Joshi and Wijeweera 1990, Ladanyi and Morel 1990, Li *et al.* 2003, Parameswaran and Jones 1981). The parameters of the springs depend on the soil stiffness; that is, when soil is frozen, the stiffness can be greatly changed. To simulate the interaction between the frozen soil and pile, an appropriate *p-y* model is essential (Yang *et al.* 2013). For sandy soils, when there is sufficient ice in the voids, cohesion will be present in the frozen soil (Arenson and Springman 2005). This means that the properties of frozen soils are similar to clay; thus, Li (2011) constructed a *p-y* curve for frozen sandy soils by using and modifying the *p-y* models for clay. Fig. 5 shows the *p-y* curve for frozen soil, which consists of a parabolic section and a constant section, as described by Eq. (11) (Yang *et al.* 2013, Yang and Zhang 2012).

$$\begin{cases} p = \frac{p_u}{2} \left( \frac{y}{y_m} \right)^{1/3} & y \leq y_u \\ p = p_u & y > y_u \end{cases} \quad (11)$$

where  $p_u$  is the ultimate resistance of frozen soil, which can be calculated by Eq. (12); and  $y_m$  is the pile deflection corresponding to half of the soil's resistance, which can be calculated by Eq. (13).  $p$  represents the soil lateral resistance per unit length of pile (kN/m), and  $y$  is the lateral deflection corresponding to  $p$ .

$$\begin{cases} p_u = q_u b \left( 1.5 + 0.25 \frac{x_{fs}}{b} \right) & 0 \leq x_{fs} \leq 12b \\ p_u = 4.5q_u b & x_{fs} > 12b \end{cases} \quad (12)$$

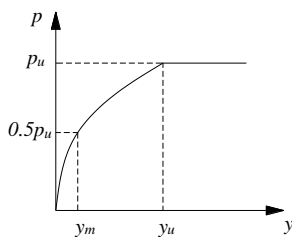


Fig. 5 The *p-y* curve for frozen soil

where  $q_u$  is the compressive strength of the frozen soil,  $b$  is the diameter of the pile, and  $x_{fs}$  is the frozen soil depth below the ground surface.

$$y_m = k_m b \quad (13)$$

where  $k_m$  is equal to the strain ( $\varepsilon_{50}$ ) at which 50% of the ultimate strength is developed. From Eq. (11),  $y_u$  can be expressed by  $y_m$  as follows

$$y_u = 8y_m \quad (14)$$

In Eqs. (11)-(14), the mechanical properties,  $q_u$  and  $k_m$ , are necessary to determine the *p-y* curves of the frozen soil at different temperatures. It has been confirmed that the strength and modulus of frozen soil increase as the temperature decreases (Sriharan *et al.* 2007). Low temperature can also cause an increase in the compressive strength and Young's modulus of concrete for the high strain rate caused by seismic action (Filiatrault and Holleran 2001). For sandy soil, through a lot of experiments and analysis, it has been found that the compressive strength is a function of the temperature of the frozen soil (Ma and Wang 2015)

$$q_u = A \left( \frac{T}{T_0} \right)^m \quad (15)$$

where  $A$  and  $m$  are the experiment parameters; and  $T_0$  is the reference temperature, which is equal to  $-1^\circ\text{C}$ .

For clay soil

$$q_u = q_0 \left( \frac{T}{T_0} \right)^j \left( \frac{t_f}{t_{f0}} \right)^n \quad (16)$$

where  $t_f$  is the failure time,  $t_{f0}=1$  min is the reference time,  $q_0$  is the compressive strength when  $t_f=1$  min and  $T=0^\circ\text{C}$ , and  $j$  and  $n$  are the empirical parameters.

In this study, the mathematical model of the seismic analysis (Eqs. (10)-(14)) is solved by the use of Newmark's method (Hu 1997), with the assistance of MIDAS software.

### 3. Numerical example

#### 3.1 Physical domain

Based on the Temporary Code for Engineering Construction of Railway in Permafrost Regions of the Qinghai-Tibet Plateau (2003) and the documented data (Cheng *et al.* 2008, Wu *et al.* 2010), a dry bridge at an elevation of 4500 m in the Qinghai-Tibet Plateau is used for the computational model, as shown in Fig. 6. The bridge selected in this study is a multi-span and simply supported reinforced concrete bridge. Double-column piers and cast-in-situ piles with the same diameters are used in the bridge. The main girder is composed of two single prefabricated reinforced concrete beams, with a T-shaped cross section. The deck width of the bridge is 4.2 m and the span is 8.5 m. A schematic diagram and the geometrical size of each component of the bridge are shown in Fig. 6. As shown in Fig. 6, girders of all the spans are supported on fixed bearing and roller bearings at ends, there are two bearings

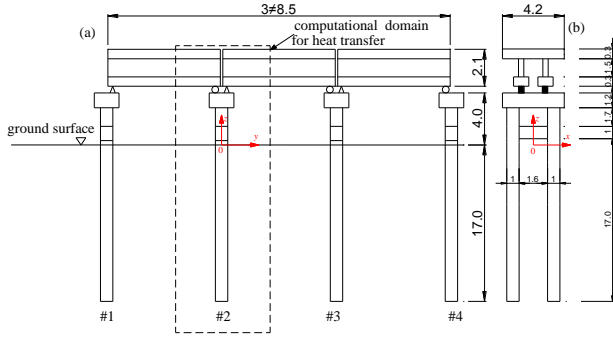


Fig. 6 Schematic diagram of the bridge (unit: m): (a) longitudinal section; (b) lateral section

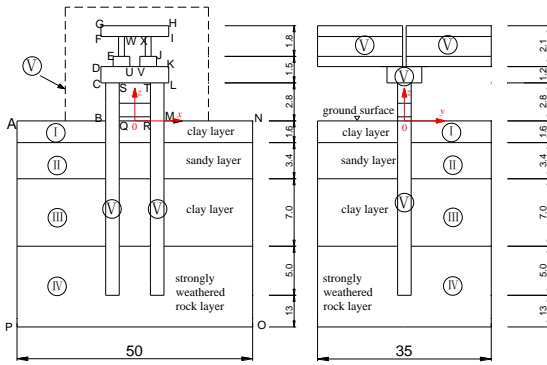


Fig. 7 Computational domain of the bridge with the soil-pile system (unit: m)

in the lateral direction because the main girder is composed of two single prefabricated reinforced concrete beams. We selected one pair of piers (#2) and the soil layers as the computational domain for the heat transfer (Fig. 7).

### 3.2 Physical parameters

In the bridge model, parts I and III are the clay layers, part II is the sandy layer, part IV is the strongly weathered mudstone layer, and part V is the concrete. The thermal parameters of the different media are listed in Table 1 (Lai *et al.* 2009a, Zhang *et al.* 2015).

According to the research of Shoukry *et al.* (2011), Sritharan *et al.* (2007), the compressive strength and the modulus of the concrete increase nearly linearly as the temperature reduces, as follows

$$f_c(T) = f_c(T > 0) - 0.13(T - 20) \quad (17)$$

$$E(T) = E(T > 0) - 0.106(T - 20) \quad (18)$$

Table 2 shows the mechanical properties of concrete at different temperatures in this analysis, based on Eqs. (17)-(18) and the Code for Design of Concrete Structures in China (GB50010-2010).

The API (American Petroleum Institute) (2005) standard is adopted in the  $p$ - $y$  curves of the unfrozen sand and clay soils, respectively. Table 3 shows the soil parameters in different temperature states for defining the  $p$ - $y$  curves, which is based on Eqs. (15)-(16) and the data from the previous research (Joshi and Wijeweera 1990, Ladanyi and

Table 1 Thermal parameters of the media in the soil-pile-bridge system

Physical variable	$\lambda_f/$ (W/m $\cdot$ °C)	$C_f/$ (J/m $^3$ $\cdot$ °C)	$\lambda_u/$ (W/m $\cdot$ °C)	$C_u/$ (J/m $^3$ $\cdot$ °C)	$L_s/$ (J/m $^3$ )
Clay layer	1.351	$1.879 \times 10^6$	1.125	$2.357 \times 10^6$	$6.03 \times 10^7$
Sandy layer	1.652	$1.941 \times 10^6$	1.421	$2.659 \times 10^6$	$4.01 \times 10^7$
Strongly weathered mudstone	1.824	$1.846 \times 10^6$	1.474	$2.099 \times 10^6$	$2.04 \times 10^7$
Concrete	1.740	$2.016 \times 10^6$	1.740	$2.016 \times 10^6$	0.0

Table 2 Mechanical properties of concrete at different temperatures

property	Temperature							
	$T > 0$ °C	0°C	-2°C	-4°C	-6°C	-8°C	-10°C	-12°C
compressive strength /Mpa	32.4	35.0	35.3	35.5	35.8	36.0	36.3	36.6
modulus /Mpa	3.45	3.66	3.68	3.70	3.73	3.75	3.77	3.79
	$\times 10^4$							

Table 3 The mechanical properties of different soils for defining  $p$ - $y$  curves

soil type	State (°C)	Friction angle (°)	Soil modulus (MPa)	Axial strain corresponding to 50% of ultimate compressive strength ( $\epsilon_{50}$ )	Unconfined ultimate compressive strength (MPa)
Clay layer	$T > 0$	—	—	0.003	0.528
	$T \leq 0$	—	—	0.0025	$q_{u1}$
Sandy layer	$T > 0$	35	16.92	—	—
	$T \leq 0$	—	—	0.005	$q_{u2}$
Strongly weathered mudstone	$T > 0$	—	—	0.002	8
	$T \leq 0$	—	—	0.001	8.5

Morel 1990, Li *et al.* 2003, Parameswaran and Jones 1981, Qi and Ma 2007), in which  $q_{u1}$  and  $q_{u2}$  for clay and sandy soils are as follows

$$q_{u1} = 0.528 \left( \frac{T}{T_0} \right)^{0.985} \left( \frac{t_f}{t_{f0}} \right)^{-0.151} \quad (19)$$

$$q_{u2} = 1.53 \left( \frac{T}{T_0} \right)^{0.699} \quad (20)$$

### 3.3 Boundary and initial conditions

#### 3.3.1 Boundary conditions

According to Qin (2002), the air temperature in the Qinghai-Tibet Plateau will increase by up to 2.6°C in the next 50 years because of climate change. The present mean annual air temperature for the bridge location is taken as -3.0°C. Based on adherent layer theory and the previous research (Lai *et al.* 2005), the boundary conditions can be specified as follows:

The air temperature

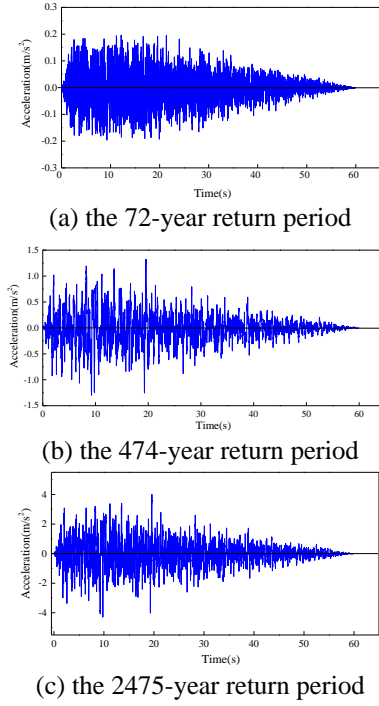


Fig. 8 Acceleration time histories of the seismic actions

$$T_{air} = -3.0 + 12 \sin\left(\frac{2\pi}{8760} t_h + \frac{\pi}{2} + \alpha_0\right) + \frac{2.6}{50 \times 365 \times 24} t_h \quad (21)$$

The temperatures at the natural ground surfaces (boundaries AB and MN, Fig. 8)

$$T_{nature-w} = -0.5 + 12 \sin\left(\frac{2\pi}{8760} t_h + \frac{\pi}{2} + \alpha_0\right) + \frac{2.6}{50 \times 365 \times 24} t_h \quad (22)$$

The temperature at the bridge surfaces with direct sunlight (boundary GH, Fig. 8)

$$T_{bridge-s} = 1.5 + 12 \sin\left(\frac{2\pi}{8760} t_h + \frac{\pi}{2} + \alpha_0\right) + \frac{2.6}{50 \times 365 \times 24} t_h \quad (23)$$

Although the solar incident angle is time-varying, shadow regions still exist under the bridge decks of east west trend. The temperatures in these regions are lower than the temperatures in the other regions with uninterrupted sunshine (boundaries QRST and UVWX, Fig. 7)

$$T_{bridge-nd} = -2.0 + 12 \sin\left(\frac{2\pi}{8760} t_h + \frac{\pi}{2} + \alpha_0\right) + \frac{2.6}{50 \times 365 \times 24} t_h \quad (24)$$

The temperatures at the lateral sides of the bridge (boundaries BCDEFG and HIJKLM, Fig. 7)

$$T_{bridge-d} = 0.7 + 12 \sin\left(\frac{2\pi}{8760} t_h + \frac{\pi}{2} + \alpha_0\right) + \frac{2.6}{50 \times 365 \times 24} t_h \quad (25)$$

where  $t_h$  is the time, and  $\alpha_0$  is the phase angle determined by the finishing time of the bridge construction. The

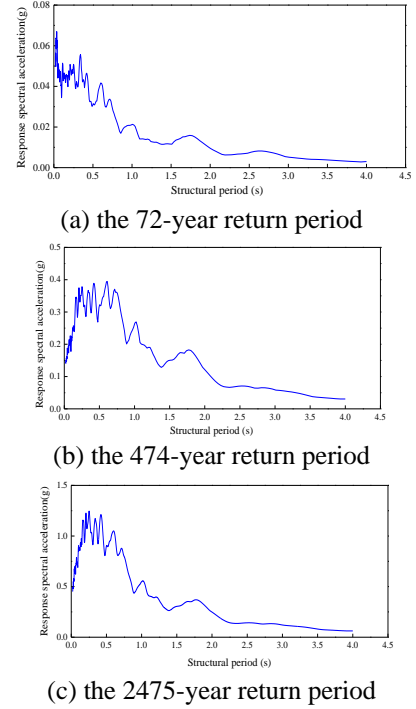


Fig. 9 Acceleration response spectra of the seismic motions

geothermal heat flux at the bottom of the domain (boundary OP, Fig. 7) is taken as  $0.06 \text{ W/m}^2$ . The lateral boundaries (AP and NO, Fig. 7) are assumed to be adiabatic.

The earthquake motions are an important boundary condition for seismic analysis. Ground motion records used in geotechnical analysis should represent the potential earthquakes at the site, i.e., magnitude, distance, source mechanism, directivity, and other effects obtained from the seismic hazard analysis (Ashtari *et al.* 2013). Because of the lack of strong seismic motion records in the selected site in the Qinghai-Tibet Engineering Corridor, the artificial seismic wave records are generated based on historical earthquakes (Cui *et al.* 2010, Wu *et al.* 2010). In order to analyze the seismic performance of the bridge under earthquakes of different intensities, three seismic motions with different return periods of 72, 474, and 2475 years, whose exceedance probabilities are 50%, 10%, and 2% in 50 years, respectively, are adopted in this study. Fig. 8 shows the acceleration time histories of the seismic motions, and Fig. 9 shows the 5% damped acceleration response spectra of the seismic motions.

The consideration of bi-directional seismic excitation is essential for the analysis and design of bridge structures (Kayhan 2016, Polycarpou *et al.* 2015). In this study, the seismic motions are input in both the longitudinal and transverse directions. The distance between the piles in the longitudinal direction is 8.5 m. As a short-span bridge, it is assumed that the ground motions at different supporting points are the same (Fan 1997), and thus the wave propagation of the seismic motions is not considered in this study.

### 3.3.2 Initial conditions

It is assumed that the bridge construction is finished on

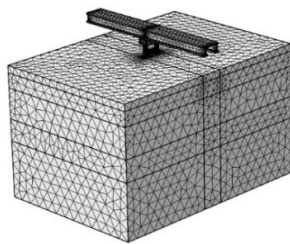
July 15. The initial temperature fields of the natural soil layers (parts I, II, III, and IV, Fig. 7) are obtained through a long-term transient solution with the upper boundary condition (Eq. (22)), without consideration of global warming. The bridge piles are cast-in-situ reinforced concrete, and the initial temperatures of the piles below the ground surface are taken as the casting temperature of the concrete, and as the mean daily air temperature on July 15 (part V, Fig. 7).

3.3.3 Simulation method

From the above it can be seen that the time scales of the heat transfer model and the dynamic analysis model are different, so that the two models can not be calculated simultaneously. Firstly, the heat transfer of the bridge-soil-pile system is simulated for 25 years after its construction. The thermal characteristics of the soil-pile system in the 5th and 25th years after its construction are analyzed from the numerical calculation results. The mechanical properties of different soils for defining *p*-*y* curves are determined by using these temperature distributions of the soil-pile system. The compressive strength and the modulus of the concrete are calculated by Eqs. (17)-(18) under different thermal conditions. Then, the dynamic characteristics of the bridge are analyzed in the 5th and 25th years. The physical models of the heat transfer and dynamic analysis are shown in Fig. 10. The seismic responses of the bridge under seismic motions with the different return periods of 72, 474, and 2475 years are calculated by the time-history method.

3.4 Numerical results and analysis

The thermal conditions have a great effect on the mechanical characteristics of the soil layers. Therefore, the interaction between the piles and the surrounding soils for a soil-pile system are significantly different under different thermal conditions. In this study, the temperature distributions of the soils around the pile of the dry bridge



(a) Physical model of heat transfer



(b) Physical model of dynamic analysis

Fig. 10 3-D numerical model of the bridge-soil-pile system

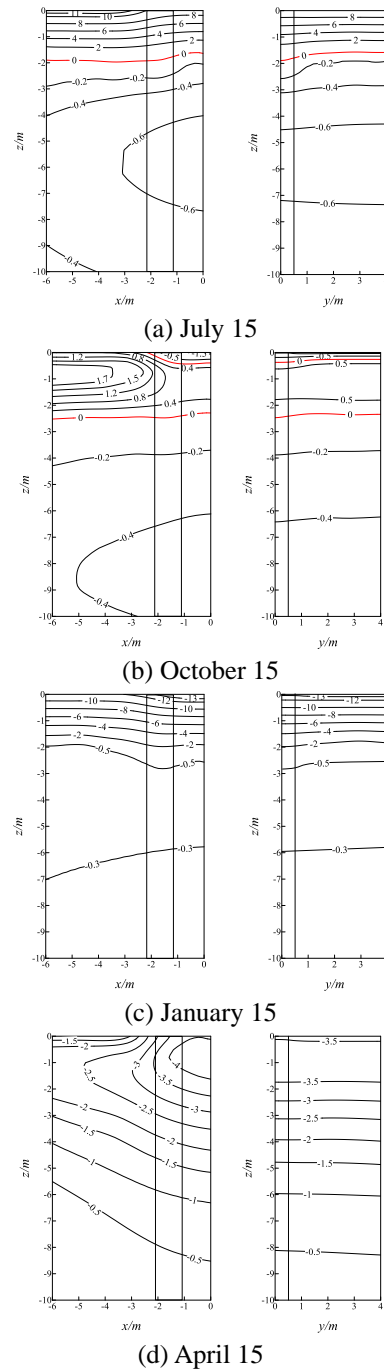


Fig. 11 Temperature distributions of the soil-pile system in 5<sup>th</sup> year after its construction

are analyzed, and then the effect on the dynamic responses of the dry bridge under seismic actions are further studied.

3.4.1 Temperature distributions

Temperature distributions in the different seasons in the 5th and 25th years after construction are shown in Figs. 11(a)-(d) and 12(a)-(d), respectively. The ground temperatures under the bridge are lower than those under the natural ground surface in all four seasons in the 5th year after construction (Fig. 11). This can be attributed to the shading effect of the bridge superstructure. From Fig. 11(b), it is found that, on October 15, the thawed depth (0°C

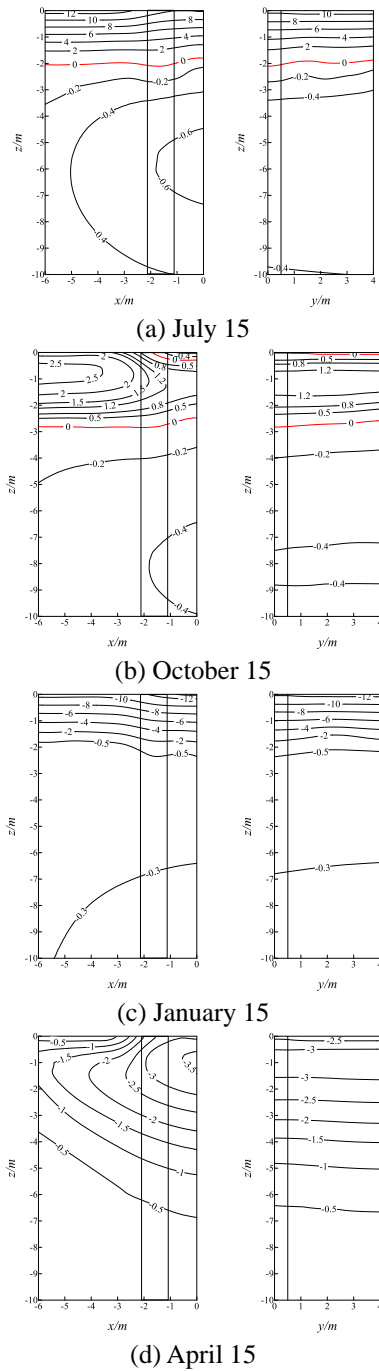


Fig. 12 Temperature distributions of the soil-pile system in 25<sup>th</sup> years after its construction

isotherm) is 2.48 m under the natural ground surface, while it is 2.29 m under the centerline of the bridge in the 5th year after construction. The difference in the thawed depths indicates that the bridge has a cooling effect on the underlying permafrost. From Fig. 12(b), it is found that, on October 15, the thawed depth (0°C isotherm) is 2.81 m under the natural ground surface, which indicates that the permafrost table declines by 0.33 m over the 20-year period. The thawed depth is 2.45 m under the centerline of the bridge in the 25th year after construction, which indicates that the permafrost table declines by 0.16 m over the 20-year period. In comparison, it is found that, although

the permafrost table in all zones declines due to global warming, the shading effect of the bridge reduces the decline of the permafrost table by 50% (0.008 m/year under the bridge and 0.017 m/year under natural ground). It can be seen that the thermal regime in the concrete pile is more sensitive to temperature change than the surrounding soil. However, the temperature distributions of the longitudinal sections in Figs. 11 and 12 show that the shading effect counteracts the negative thermal disturbance of the concrete piles on the surrounding permafrost.

From the above analysis, it is found that the temperature distributions of the ground in a permafrost region are significantly different in the different seasons, especially in the active layer. As for the permafrost with a dry bridge constructed on it, the temperature distributions are changed by the difference in the heat transfer between concrete and soil, and most importantly by the shading effect of the bridge deck. In this study, the temperature rise caused by global warming is considered, so that the permafrost table declines and the active layer thickens in the 25th year after construction (Fig. 12) compared with the 5th year after construction (Fig. 11). These temperature variations and distributions of the soil-pile system have a significant effect on the dynamic responses of the dry bridge under seismic action, which are analyzed in detail in the following.

### 3.4.2 Analysis of the structural period

Although structural period analysis is not related to loading type, it is very important to dynamic analysis. Usually it is the first and necessary step in dynamic analysis, including natural frequency and mode shape analyses to characterize the basic dynamic behavior, as an indication of how structures will respond to dynamic loading (Ngo-Tran *et al.* 2007). The boundary conditions have great effects on the free vibration characteristic of bridge, the most importance of which is the interaction relationship of piles with the surrounding soils.

Modal analysis is conducted in four different thermal conditions (i.e., July 15, October 15, January 15 and April 15) in 5th and 25th years after the construction of the bridge, and the first three natural frequencies are obtained from modal analysis. Because of the different temperature distributions in the four reasons, the warm (i.e., July 15, October 15) and cold seasons (i.e., January 15 and April 15) can both be included in the analysis. From the temperature distributions, we know that the active layer is thawed in the warm seasons, while, all the soil layers are frozen in cold seasons. The frequency values in different thermal conditions are shown in Tables 4 and 5. The results show that there is an obvious difference in the natural vibration

Table 4 Modal frequencies for x direction of the dry bridge

Modes	5th year after its construction				25th year after its construction			
	July 15 $\omega$ (Hz)	October 15 $\omega$ (Hz)	January 15 $\omega$ (Hz)	April 15 $\omega$ (Hz)	July 15 $\omega$ (Hz)	October 15 $\omega$ (Hz)	January 15 $\omega$ (Hz)	April 15 $\omega$ (Hz)
1	2.302	2.421	2.775	2.572	2.269	2.267	2.767	2.655
2	4.680	4.806	5.223	5.010	4.636	4.618	5.217	5.100
3	5.811	6.053	7.005	6.459	5.757	5.733	6.985	6.681

Table 5 Modal frequencies for y direction of the dry bridge

Modes	5th year after its construction				25th year after its construction			
	July	October	January	April	July	October	January	April
	$15 \omega$ (Hz)	$15 \omega$ (Hz)	$15 \omega$ (Hz)	$15 \omega$ (Hz)	$15 \omega$ (Hz)	$15 \omega$ (Hz)	$15 \omega$ (Hz)	$15 \omega$ (Hz)
1	2.288	2.406	2.756	2.555	2.256	2.254	2.748	2.637
2	2.316	2.436	2.795	2.589	2.282	2.280	2.787	2.673
3	5.736	5.963	6.461	6.210	5.647	5.641	6.454	6.317

characteristics of bridge under the cold and warm seasons: the natural vibration frequency of the bridge under cold seasons is higher than that in warm seasons. It also shows that the global warming has a relatively little impact on site characteristics in warm seasons, but it had a larger impact on the site characteristics in cold seasons because the mechanical properties of frozen soil are closely related to the temperature (Lai *et al.* 2009b). Based on microseism tests at the typical permafrost sites along the Qinghai-Tibet Railway, Wu *et al.* (2008) summarized that the vertical predominant frequencies of permafrost sites are between 3.3 Hz and 4.8 Hz, and the horizontal predominant frequencies are between 2.3 Hz and 4.7 Hz. It is well known that every site has a specific seismic response at which the ground shaking can be amplified with specific frequency, and if it matches with the fundamental frequency of the man-made structures, then there may be maximum probability of damage due to resonance of frequency (Singh *et al.* 2014). In the permafrost regions, it is found that the difference of frequencies is considerable between the cold and warm seasons, and concluded that the unfrozen active layer in permafrost site plays a dominant role in amplifying ground motion components with relatively longer period (lower frequency) and in shifting the predominant period to longer period. However the frozen layer attenuates ground motion components with relatively shorter period (higher frequency) (Yang *et al.* 2011). It is known that the natural frequency is related to the stiffness and mass of the structure, and large stiffness results in high frequency. From Tables 4 and 5, it is found that the natural frequencies for  $x$  direction are larger than that for  $y$  direction, which indicated that the  $x$  direction of the bridge is more vulnerable than the  $y$  direction under the seismic action. The results also show that the natural frequencies of the bridge in warm seasons are closer to the characteristic frequency (2.3-4.8 Hz) of the site than that in cold seasons. Therefore, it is concluded that the bridge constructed in permafrost regions is easier to be damaged in warm seasons than in cold seasons when an earthquake occurs.

### 3.4.3 Analysis of the seismic responses

The thawing depth is the largest on October 15 and the lowest temperature occurs on January 15. Therefore, the two dates (i.e., October 15 and January 15) are selected as research objectives. Here, pile #2 is selected as an example, and the envelopes of the lateral displacement, shear force, and bending moment of the pile with depth on October 15 and January 15 in the 5th year after construction are shown in Figs. 13-18. In the figures, positive values of depth represent above the ground surface, and negative below.

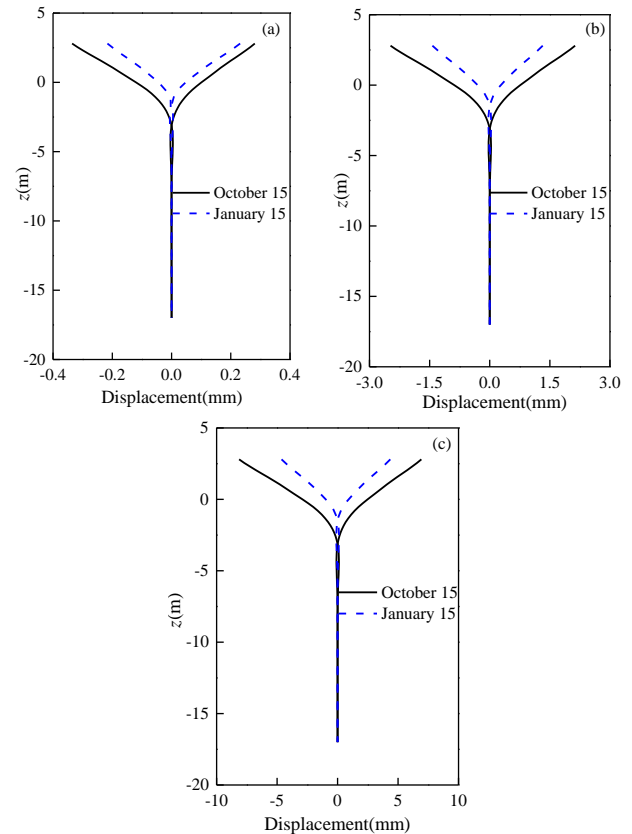


Fig. 13 Displacements of pile in  $x$  direction under seismic actions with (a) 72-year return period; (b) 474-year return period; and (c) 2475-year return period

Figs. 13 and 14 show the displacements in the lateral ( $x$ ) and longitudinal ( $y$ ) directions, respectively. The displacement in the lateral ( $x$ ) direction is far less than that in the longitudinal ( $y$ ) direction under the same seismic action, which illustrates that the displacement in the  $y$  direction is the main control factor of pile deformation for the multi-span and simply supported beam bridge. The difference between the two directions is partially due to the plane frame structure constructed by the double-column piles and the tied beam between them on the  $xz$  plane, as shown in Fig. 7. The larger natural frequencies indicated that the bridge system has greater stiffness in the  $x$  direction than in the  $y$  direction. Therefore, the greater stiffness leads to smaller displacement of the column in the  $x$  direction than in the  $y$  direction.

The displacement in the two directions increases with the increase of the seismic intensity (return period). In Fig 14, as the displacement on October 15 increases from 1.4 to 11.6 mm as the return period of the seismic motion increases from the 72- to the 474-year action, the difference is 10.2 mm. The corresponding difference between the 474- and 2475-year actions is 24.7 mm. This is because the pile element has nonlinear but elastic behavior, where a large increase in strain occurs with a modest increase in stress once the strain of the materials increases to a critical value.

It is also found that the displacements in the  $x$  and  $y$  directions on October 15 are larger than those on January 15 in Figs. 13 and 14, which is due to the freeze-thaw state of

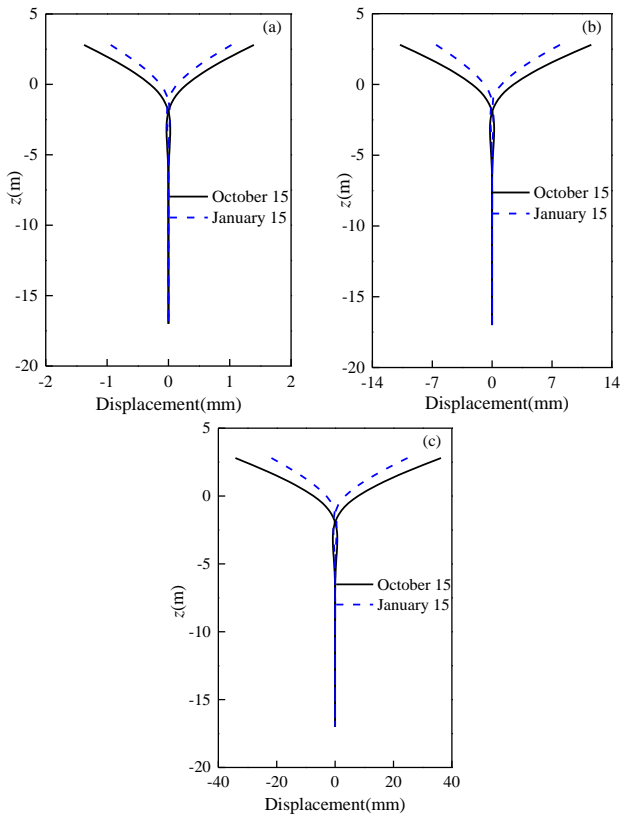


Fig. 14 Displacements of pile in  $y$  direction under seismic actions with (a) 72-year return period; (b) 474-year return period; and (c) 2475-year return period

the active layer. Taking the displacements in Fig. 14(c) as an example, the maximum displacements in the  $x$  direction are 4.4 mm and 6.9 mm on January 15 and October 15, respectively, and the corresponding displacements in the  $y$  direction are 24.8 mm and 36.3 mm, respectively. Compared with the unfrozen active layer on October 15, the frozen active layer on January 15 results in an approximately 32% decrease in maximum displacement, which is about 50% of the displacement at the ground surface ( $z=0$  m). The other figures show similar characteristics to Fig. 14(c).

Figs. 15 and 16 show the shear force down the length of the pile in the  $x$  and  $y$  directions under the 72-, 474-, and 2475-year return period seismic actions. From Fig. 15, the shear forces in the  $x$  direction change only slightly above the ground surface, while, below the ground surface, they quickly increase to the maximum and then decrease sharply on January 15, and change more gently on October 15 at the same time under the same seismic action. The peak shear force on the pile below the ground surface on January 15 is larger than that on October 15, which is due to the frozen active layer. Actually, the unfrozen active layer in the warm season (i.e., October 15) largely absorbs seismic energy by deformation, but the frozen active layer in the cold season (i.e., January 15) confines the pile deformation (Figs. 13 and 14). The depth of the peak shear force in the  $x$  direction on January 15 is always deeper than that on October 15. Thus, it can be concluded that the unfrozen active layer also changes the location of the peak shear force.

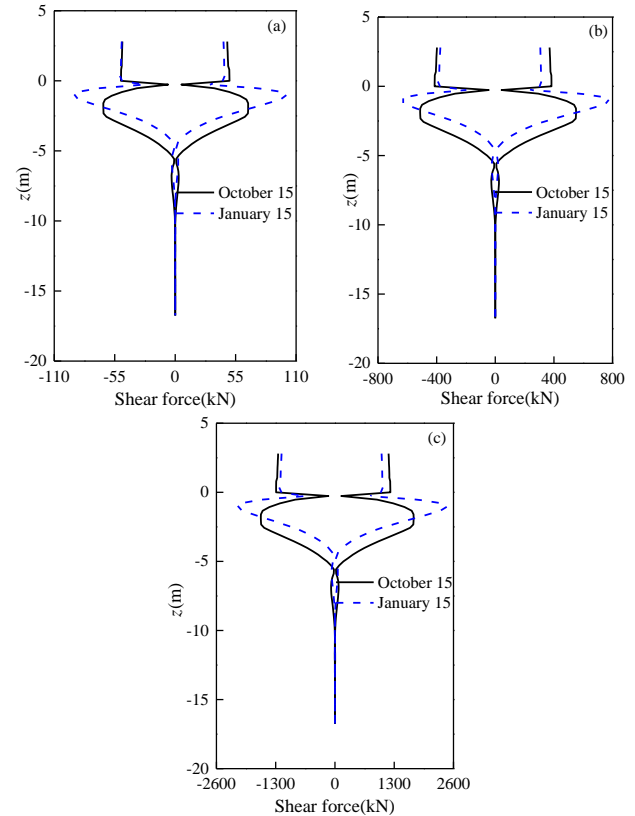


Fig. 15 Shear force of pile in  $x$  direction under seismic actions with (a) 72-year return period; (b) 474-year return period; and (c) 2475-year return period

From Figs. 15 and 16, it can also be seen that the shear forces of the two different directions ( $x$  and  $y$  directions) show big differences in magnitude and distribution under the same seismic action. The peak value of the shear force in the lateral direction ( $x$  direction) occurs below the ground surface, but it occurs above the ground surface in the longitudinal direction ( $y$  direction). There is little difference in the shear forces between the  $x$  and  $y$  directions above the ground surface, but the difference becomes greater below the ground surface, and the peak shear force in the  $x$  direction is about six times larger than in the  $y$  direction. It is known that the shear forces in the column are related to the inertial forces transmitted from the superstructures, which is further related to the natural frequency and the tributary superstructure mass on the column. For a simply supported bridge, the tributary superstructure mass on the column for both longitudinal and lateral directions should be almost the same (about one-span mass). The tributary superstructure mass is shared by the two columns piles in  $y$  direction, whereas the  $x$ -direction involves only one column-piles systems. Furthermore, the natural frequencies of the bridge (Tables 4 and 5) for  $x$  direction are larger than that for  $y$  direction. As a result, the inertial forces in the column transmitted from the superstructures for  $x$  direction are larger than that for  $y$  directions. Therefore, this suggests that the anti-shear capacity of the piles under the ground surface in the  $x$  direction should be enhanced in the design of dry bridges in permafrost regions.

Similar to the displacement characteristics, the value of

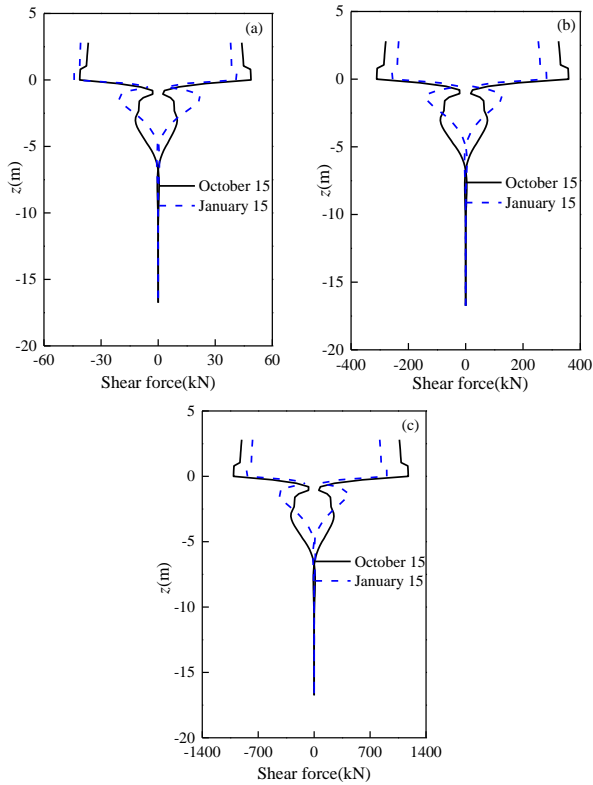


Fig. 16 Shear force of pile in y direction under seismic actions with (a) 72-year return period; (b) 474-year return period; and (c) 2475-year return period

the shear force increases when the seismic action changes from the 72-year return period to the 2475-year return period, but the locations of the noticeable shear force show no obvious changes with the increase of the return period of the seismic action.

The bending moments of the two directions in the 72-, 474-, and 2475-year return period seismic motions are given in Figs. 17 and 18. The bending moments of the x direction (on the y-z plane, Fig. 7(b)) are more complicated in distribution than those of the y direction (on the x-z plane, Fig. 7(a)) under the same seismic action, but they are much smaller in value. For different types of structure, to some extent, the force and deformation characteristics of the system are different. The tied beam between the two piles changes the bending moment distribution in the x direction, and makes it more complicated than that in the y direction. In comparison, it is found that the maximum bending moment in the y direction is about four times larger than in the x direction at the same depth, so that bending failure of the pile will first appear in the y direction under seismic action. The bending stiffness in the y direction (on the x-z plane) must therefore be strengthened in the design of the piles.

The different temperature distributions of the soil layer, especially the active layer, also change the value and location of the zero and peak bending moment in different seasons. For the bending moment in the y direction, the value of the peak bending moment on October 15 is smaller than that on January 15, and the location of the peak bending moment on October 15 is lower than that on

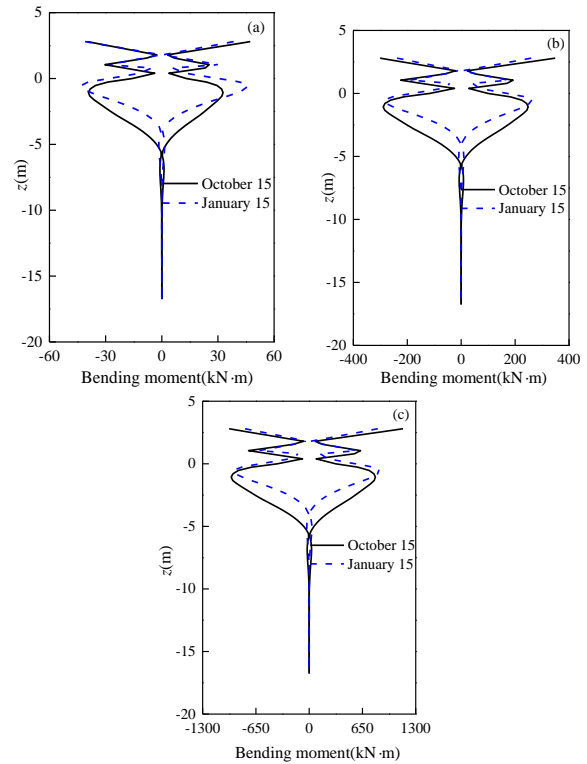


Fig. 17 Bending moment of pile in x direction under seismic actions with (a) 72-year return period; (b) 474-year return period; and (c) 2475-year return period

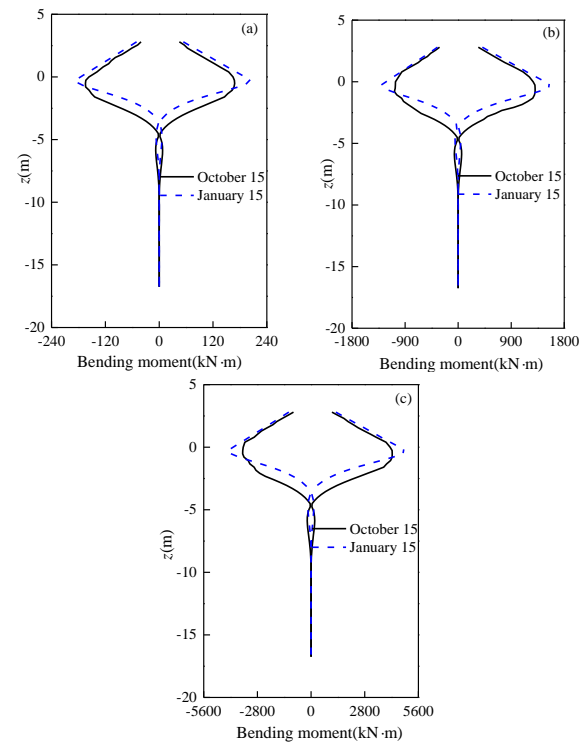


Fig. 18 Bending moment of pile in y direction under seismic actions with (a) 72-year return period; (b) 474-year return period; and (c) 2475-year return period

January 15. For the seismic action with a 72-year return period in Fig. 18a, the peak bending moments are 202.2

kN·m on January 15 and 167.4 kN·m on October 15, a decrease of 17%, and the depth of the peak bending moment is about 0.3 m on January 15 and about 0.5 m on October 15, an increase of 40%. The bending moments under other seismic actions (Figs. 18(b) and (c)) have similar characteristics.

It is known that the increased thickness of active layer (induced by global warming) on October 15 (Figs. 11(b) and 12(b)) weakens the soil strength and rigidity, but the unfrozen soil layer can play a role in passive energy dissipation under seismic action, compared with the frozen soil layer in the cold seasons.

It is found that the temperature distributions, especially the freeze-thaw state in permafrost regions, have a significant influence on the lateral displacement, shear force, and bending moment of piles under seismic actions, which is confirmed in Figs. 13-18. Energy dissipation as a means of reducing the seismic response of structures has become a popular topic among researchers and structural engineers (Abdel and Toshiro 2013). Damping is an important way of energy dissipation under seismic action, and foundation (soil layer) damping is as efficient as the structural passive energy dissipation devices, and normally works better than structural damping (Crouse and McGuire 2001, Gajan and Saravanathibban 2011). The frozen active layer in warm seasons enhances the strength and stiffness of the soil layer, and confines the relative displacement between pile and soil in cold seasons. However, the increased stiffness of the frozen soil reduces the energy dissipation of the soil layer compared to the unfrozen active layer.

It is also found that the depth of the dynamic responses along the pile do not exceed 8 m, which is less than half of the length of the pile. Therefore, if the seasonal change of the active layer is not considered, the piles may fail to prevent bridge damage from earthquakes in permafrost regions. The thermal regime of the permafrost surrounding the pile is changed due to global warming (Figs. 11 and 12), so that the dynamic responses of the bridge change accordingly. However, the results are not discussed in detail in this paper.

#### 4. Conclusions

To evaluate the thermal disturbance of bridges on the surrounding permafrost and the effect of the active layer on the seismic responses of bridges in permafrost regions, a dry bridge constructed in the Qinghai-Tibet Railway is analyzed. A numerical model considering the soil-pile interactions is presented to investigate the seismic response of the bridge in permafrost region. Some conclusions can be drawn:

- The thermal regime of the bridge-pile-soil system are analyzed, with consideration of the effect of global warming. It is shown that the shading effect of the bridge decks can counteract the negative thermal disturbance of the concrete piles on the surrounding permafrost.
- In the analysis of the dynamic characteristics of the bridge, seismic actions with different intensities (72-,

474-, and 2475-year return periods) are selected to analyze the seismic behavior by using a time-history analysis method, with consideration of bi-directional seismic excitation. The results show that the freeze-thaw state of the active layer in permafrost regions has a significant impact on the dynamic responses, including the lateral displacement, shear force, and bending moment of the bridge piles in the two orthogonal directions (i.e., longitudinal and lateral directions).

- It is found that the frozen active layer in cold seasons confines the deformation of the bridge pile, but it also increases the shear force and bending moment due to the reduced energy dissipation, compared with the unfrozen active layer in warm seasons.

It is therefore concluded that the effect of the thermal regime of the soil layers, especially the active layer, cannot be ignored in the design and construction of dry bridges in permafrost regions.

#### Acknowledgements

This research was supported by the National Natural Science Foundation of China (Grant No. 41471063, 51468031 and 51768036), the 100-Talent Program of the Chinese Academy of Sciences (Granted to Dr. Mingyi Zhang), and the Program of the State Key Laboratory of Frozen Soil Engineering (Grant No. SKLFSE-ZT-23), and the STS Program of the Chinese Academy of Sciences (Grant No. HHS-TSS-ST-1502).

#### References

- Abdel, R.S.E. and Toshiro, H. (2013), "Energy dissipation system for earthquake protection of cable-stayed bridge towers", *Earthq. Struct.*, **5**(5), 657-678.
- Allotey, N. and El Naggar, M.H. (2008), "Generalized dynamic Winkler model for nonlinear soil-structure interaction analysis", *Can. Geotech. J.*, **45**(4), 560-573.
- Anisimov, O.A., Shiklomanov, N.I. and Nelson, F.E. (1997), "Global warming and active-layer thickness: results from transient general circulation models", *Global Planet. Change*, **15**(3), 61-77.
- API (American Petroleum Institute) (2005), Recommended Practice for Planning, Designing and Constructing Fixed Offshore Platforms: Working Stress Design, American Petroleum Institute.
- Arenson, L.U. and Springman, S.M. (2005), "Mathematical descriptions for the behaviour of ice-rich frozen soils at temperatures close to 0°C", *Can. Geotech. J.*, **42**(2), 431-442.
- Ashtari, P., Ghasemi, S.H. and Ashtari, P. (2013), "Seismic design of structures using a modified non-stationary critical excitation", *Earthq. Struct.*, **4**(4), 383-396.
- Carcione, J.M. and Seriani, G. (1998), "Seismic and ultrasonic velocities in permafrost", *Geophys. Prosp.*, **46**(4), 441-454.
- Cervera, M., Faria, R., Oliver, J. and Prato, T. (2002), "Numerical modelling of concrete curing, regarding hydration and temperature phenomena", *Comput. Struct.*, **80**(18-19), 1511-1521.
- Che, A.L., Wu, Z.J. and Wang, P. (2014), "Stability of pile foundations base on warming effects on the permafrost under earthquake motions", *Soil. Found.*, **54**(4), 639-647.
- Cheng, G., Sun, Z. and Niu, F. (2008), "Application of the roadbed

- cooling approach in Qinghai-Tibet railway engineering”, *Cold Reg. Sci. Technol.*, **53**(3), 241-258.
- Cheng, G., Wu, Q. and Ma, W. (2008), “Innovative designs of permafrost roadbed for the Qinghai-Tibet Railway”, *Sci. China Ser. E: Technol. Sci.*, **52**(2), 530-538.
- Cheng, G.D. (2003), “Construction of Qinghai-Tibet Railway with cooled roadbed”, *China Railw. Sci.*, **24**(3), 1-4. (in Chinese)
- Crouse, C.B. and McGuire, J. (2001), “Energy dissipation in soil-structure interaction”, *Earthq. Spectra*, **17**(2), 235-259.
- Crowther, G.S. (1990), “Analysis of laterally loaded piles embedded in layered frozen soil”, *J. Geotech. Eng.*, **116**(7), 1137-1152.
- Fan, L.C. (1997), *Seismic Design of Highway Bridge*, Huajie International Publishing Co. Limited.
- Filiatrault, A. and Holleran, M. (2001), “Stress-strain behavior of reinforcing steel and concrete under seismic strain rates and low temperatures”, *Mater. Struct.*, **34**(4), 235-239.
- Gajan, S. and Saravanathiiban, D.S. (2011), “Modeling of energy dissipation in structural devices and foundation soil during seismic loading”, *Soil Dyn. Earthq. Eng.*, **31**(8), 1106-1122.
- GB50010 (2010), Code for Design of Concrete Structures, China Building Industry Press, Beijing. (in Chinese)
- Ge, X., Yang, Z., Still, B. and Li, Q. (2012), “Experimental study of frozen soil mechanical properties for seismic design of pile foundations”, *Cold Regions Engineering 2012: Sustainable Infrastructure Development in a Changing Cold Environment*.
- Geng, F., Ding, Y., Song, J., Li, W. and Li, A. (2014), “Passive control system for seismic protection of a multi-tower cable-stayed bridge”, *Earthq. Struct.*, **6**(5), 495-514.
- Han, Q., Dong, H., Du, X. and Zhou, Y. (2015), “Pounding analysis of RC bridge considering spatial variability of ground motion”, *Earthq. Struct.*, **9**(5), 1029-1044.
- Hu, N. (1997), “A solution method for dynamic contact problems”, *Comput. Struct.*, **63**(6), 1053-1063.
- Jin, H., Li, S., Cheng, G., Shaoling, W. and Li, X. (2000), “Permafrost and climatic change in China”, *Glob. Planet. Change*, **26**(4), 387-404.
- Joshi, R. and Wijeweera, H. (1990), “Post peak axial compressive strength and deformation behavior of fine-grained frozen soils”, *Proceedings of the Fifth Canadian Permafrost Conference*, 317-325.
- Kayhan, A.H. (2016), “Scaled and unscaled ground motion sets for uni-directional and bi-directional dynamic analysis”. *Earthq. Struct.*, **10**(3), 563-588.
- Klemczak, B. and Knoppik-Wróbel, A. (2011), “Numerical analysis of early-age thermal and moisture effects in RC wall”, *Proceedings of the 7th International Conference in Analytical Models and New Concepts in Concrete and Masonry Structures*, Kraków.
- Ladanyi, B. and Morel, J.F. (1990), “Effect of internal confinement on compression strength of frozen sand”, *Can. Geotech. J.*, **27**(1), 8-18.
- Lai, Y., Jin, L. and Chang, X. (2009b), “Yield criterion and elastoplastic damage constitutive model for frozen sandy soil”, *Int. J. Plast.*, **25**, 1177-1205.
- Lai, Y.M., Zhang, M.Y. and Li, S.Y. (2009a), *Theory and Application of Cold Regions Engineering*, Science Press, Beijing. (in Chinese)
- Lai, Y.M., Zhang, X.F., Xiao, J.Z., Zhang, S.J. and Liu, Z.Q. (2005), “Nonlinear analysis for frost-heaving force of land bridges on Qing-Tibet Railway in cold regions”, *J. Therm. Stress.*, **28**(3), 317-331.
- LeBlanc, A.M., Fortier, R., Allard, M., Cosma, C. and Buteau, S. (2004), “Seismic cone penetration test and seismic tomography in permafrost”, *Can. Geotech. J.*, **41**(5), 796-813.
- Li, H.P., Zhu, Y.L. and Pan, W.D. (2003), “Uniaxial compressive strength of saturated frozen silt”, *Proceedings of the 8th International Conference on Permafrost*, 679-684.
- Li, Q. (2011), “Effect of frozen soils on the seismic behavior of highway bridge foundation”, M.S. University of Alaska Anchorage. Available from ProQuest Dissertations & Theses A&I, ProQuest Dissertations and Theses A&I, The Sciences and Engineering Collection.
- Ma, W. and Wang, D. (2015), *Mechanics of Frozen Soil*, Science Press, Beijing, China. (in Chinese)
- Ngo-Tran, T.L., Hayashikawa, T. and Hirasawa, H. (2007), “Improving free vibration characteristics of horizontally curved twin I-girder bridges”, *Kozo Kagaku Ronbunshu. A (J. Struct. Eng. A)*, **53A**, 268-276.
- Parameswaran, V.R. and Jones, S.J. (1981), “Triaxial testing of frozen sand”, *J. Glaciol.*, **27**(95), 147-155.
- Polycarpou, P.C., Papaloizou, L., Komodromos, P. and Charmpis, D.C. (2015) “Effect of the seismic excitation angle on the dynamic response of adjacent buildings during pounding”, *Earthq. Struct.*, **8**(5), 1127-1146.
- Qi, J. and Ma, W. (2007), “A new criterion for strength of frozen sand under quick triaxial compression considering effect of confining pressure”, *Acta Geotechnica*, **2**(2), 221-226.
- Qin, D.H. (2002), *The Comprehensive Evaluating Report on the Environment Evolution in West China*, Science Press, Beijing. (in Chinese)
- Shao, G. and Jiang, L. (2014), “Experimental investigations of the seismic performance of bridge piers with rounded rectangular cross-sections”, *Earthq. Struct.*, **7**(25), 463-484.
- Shoukry, S.N., William, G.W., Downie, B. and Riad, M.Y. (2011), “Effect of moisture and temperature on the mechanical properties of concrete”, *Constr. Build. Mater.*, **25**(2), 688-696.
- Singh, A.P., Annam, N. and Kumar, S. (2014), “Assessment of predominant frequencies using ambient vibration in the Kachchh region of western India: implications for earthquake hazards”, *Nat. Hazard.*, **73**, 1291-1309.
- Sritharan, S., Suleiman, M.T. and White, D.J. (2007), “Effects of seasonal freezing on bridge column-foundation-soil interaction and their implications”, *Earthq. Spectra*, **23**(1), 199-222.
- Suleiman, M., Sritharan, S. and White, D. (2006), “Cyclic lateral load response of bridge column-foundation-soil systems in freezing conditions”, *J. Struct. Eng.*, **132**(11), 1745-1754.
- Wilson, E.L. (1999). *Three Dimensional Static and Dynamic Analysis of Structures*, Computers and Structures.
- Wotherspoon, L.M., Sritharan, S. and Pender, M.J. (2010), “Modelling the response of cyclically loaded bridge columns embedded in warm and seasonally frozen soils”, *Eng. Struct.*, **32**(4), 933-943.
- Wu, Q., Zhang, T. and Liu, Y. (2010), “Permafrost temperatures and thickness on the Qinghai-Tibet Plateau”, *Glob. Planet. Change*, **72**(1-2), 32-38.
- Wu, Z., Che, A.L., Tuo, G. and Wang, P. (2010), “Test study and numerical analysis of seismic response of pile foundation of bridge at permafrost regions along Qinghai-Tibet Railroad”, *Rock Soil Mech.*, **31**(11), 3516-3524. (in Chinese)
- Wu, Z., Wang, L., Sun, J., Xu, S. and Cheng, G. (2008), “Characteristics of microseism at typical permafrost sites in Qinghai-Tibet plateau”, *Chin. J. Rock Mech. Eng.*, **27**, 2316-2323.
- Xiong, F. and Yang, Z. (2008), “Effects of seasonally frozen soil on the seismic behavior of bridges”, *Cold Reg. Sci. Technol.*, **54**(1), 44-53.
- Xu, X., Chen, W., Ma, W., Yu, G. and Chen, G. (2002), “Surface Rupture of the Kunlunshan Earthquake (Ms 8.1), Northern Tibetan Plateau, China”, *Seismol. Res. Lett.*, **73**(6), 884-892.
- Yang, Z., Dutta, U., Xu, G., Hazirbaba, K. and Marx, E.E. (2011), “Numerical analysis of permafrost effects on the seismic site response”, *Soil Dyn. Earthq. Eng.*, **31**(3), 282-290.
- Yang, Z., Dutta, U., Zhu, D., Marx, E. and Biswas, N. (2007),

- “Seasonal frost effects on the soil-foundation-structure interaction system”, *J. Cold Reg. Eng.*, **21**(4), 108-120.
- Yang, Z.H., Zhang, X.Y., Ge, X.X. and Marx, E.E. (2013), “Application of p-y approach in analyzing pile foundations in frozen ground overlying liquefiable soils”, *Sci. Cold Arid Reg.*, **5**(4), 368-376.
- Yang, Z.J. and Zhang, X. (2012), “Seismic performance and design of bridge foundations in liquefiable ground with a frozen crust”, University of Alaska Anchorage, School of Engineering, Washington, DC.
- Zhang, M., Lai, Y., Li, D., Tong, G. and Li, J. (2012), “Numerical analysis for thermal characteristics of cinderblock interlayer embankments in permafrost regions”, *Appl. Therm. Eng.*, **36**, 252-259.
- Zhang, M., Pei, W., Zhang, X. and Lu, J. (2015), “Lateral thermal disturbance of embankments in the permafrost regions of the Qinghai-Tibet Engineering Corridor”, *Nat. Hazard.*, **78**(3), 2121-2142.

KT